Composites: Part B 54 (2013) 278–288

Contents lists available at SciVerse ScienceDirect

Composites: Part B

journal homepage: www.elsevier.com/locate/compositesb

Strength analysis of particulate polymers

V. Birman [a,b,*], K. Chandrashekhara [b], M.S. Hopkins [c], J.S. Volz [c]

[a] Missouri University of Science and Technology, Engineering Education Center, 12837 Flashing Meadows Drive, St. Louis, MO 63131, United States
[b] Missouri University of Science and Technology, Department of Mechanical and Aerospace Engineering, Rolla, MO 65409, United States
[c] Missouri University of Science and Technology, Department of Civil, Architectural and Environmental Engineering, Rolla, MO 65409, United States

ARTICLE INFO

Article history:
Received 21 February 2013
Accepted 1 May 2013
Available online 15 May 2013

Keywords:
A. Particle-reinforcement
B. Strength
B. Stress concentration
C. Micro-mechanics

ABSTRACT

Impregnating polymeric matrix with stiff particles may significantly improve structural response of a composite material. Such improvements have to be weighed against the effects of the stress concentration at the particle–matrix interface that influence local strength and toughness. In the present paper we elaborate on the issue of local stresses and strength in particulate polymer matrix composites considering polyurethane matrix impregnated with alumina particles in numerical examples. The parametric analysis presented in the paper is concerned with the effects of the particle volume fraction and the particle-to-matrix stiffness ratio on the local stresses and initial damage. We also discuss the resilience of the impregnated polyurethane, i.e. the density of energy necessary to produce initial damage. The approach to the analysis of fracture in the composite with initial damage is discussed accounting for available experimental observations. Three scales of fracture corresponding to different phases of the development and propagation of the crack are identified, including microfracture at the particle–matrix interface and mesofracture limited to the matrix surrounding the particle. While these scales of fracture should be analyzed by numerical methods, macrofracture that occurs after the crack "emerged" from the representative unit cell where it originated can be considered using available analytical techniques. The methodology of the stress analysis of a particulate material consisting of an incompressible hyperelastic matrix and much stiffer elastic particles is also proposed in the paper.

1. Introduction

Polymeric composites incorporating particles or short fibers are attractive due to their good mechanical properties that are often achieved at a relatively low cost. Besides particulate and short-fiber composite materials, the properties of polymeric foams may also be improved if they are impregnated by particles [1].

Numerous studies have been dedicated to the analysis of stiffness of particulate and short-fiber composites. They include various analytical, semi-empirical and numerical models. While the comprehensive analysis of relevant studies is outside the scope of this paper, we mention a number of reviews, such as [2–5]. The stiffness of particulate hyperelastic elastomers has also been studied, e.g., [6,7]. The studies considering the strength of particulate composites are less prominent, ranging from finite element analyses [8,9] to semi-empirical investigations attempting to account for the adhesion of particles to matrix, stress concentration and interfacial shear strength [10,11]. The attempts to account for the effects of the size of particles (e.g., [12]) and the presence of voids [13] on the strength have also been undertaken.

The effect of spherical particles on the crack propagation in the composite material has been extensively studied in the framework of linear elastic fracture mechanics resulting in the closed-form expressions for the stress intensity factors (e.g., review [14]). The mechanisms include crack deflection and tilting, crack trapping that results in bowing of the front of the crack, and debonding of particles from the matrix accompanied with sliding energy dissipation along the interface [15–18].

In this paper we present a parametric stress analysis of a particulate composite consisting of a polymeric matrix reinforced with spherical elastic particles (polyurethane impregnated with alumina powder is considered in examples). The analysis includes the determination of stresses at the interface and in the matrix, just outside the particles, where the stress concentration results in elevated stresses. We consider the entire circumference of the particle to account for the three-dimensional state of stress and specify the location and magnitude of the largest principal and von Mises stresses. The stress analysis is conducted by the Mori–Tanaka technique [19,20] that was shown in good agreement with experimental and numerical data as well as with the self-consistent method for the range of particle volume fraction below 30% (e.g., [1,21]).

The initial failure observed in experiments on vinylester matrix composites reinforced by spherical glass or alumina particles was a

* Corresponding author. Tel.: +1 314 835 9818; fax: +1 314 835 9815.
E-mail address: vbirman@mst.edu (V. Birman).

1359-8368/$ - see front matter © 2013 Elsevier Ltd. All rights reserved.
http://dx.doi.org/10.1016/j.compositesb.2013.05.009

debonding of the particles from the matrix at the apex ("pole") of the particle [12] and the propagation of the interface debond crack, followed with cracking in the matrix originating from the debond crack. The distribution of the stresses determined in our analysis for polyurethane-matrix, alumina-particle composites confirms the observed location of the initial damage.

As shown in the paper, knowing the initial failure load, the resilience of the particulate material can be compared with that of the pristine matrix material. The analysis of fracture reflecting the sequence reported in [12] involves three phases: microfracture corresponding to the origination and propagation of the initial crack along the particle–matrix interface, mesofracture when the crack kinks off the interface and propagates in the matrix of the representative unit cell (RUC) consisting of a single particle surrounded with the matrix, and finally, macrofracture concerned with the propagation of a "mature" crack whose length exceeds the scale of RUC. The peculiarities of the microfracture and mesofracture formulations including the spherical shape of the particle–matrix interface and stresses that vary both along the interface and within the matrix necessitate a numerical analysis. Macrofracture can be analyzed by one of the available theories developed for particulate composites. In particular, the solution by Bower and Ortiz accounts for several known effects of particles on fracture [18].

A separate section of the paper introduces the approach to the stress analysis of the material consisting of stiff particles embedded within an incompressible hyperelastic matrix. The solution represents a combination of the Mori–Tanaka stress and stiffness analysis with the Bergstrom–Boyce model of a hyperelastic material with rigid particles [6]. The stiffness of the particulate material and that of the matrix are represented by tangential tensors dependent on the strain in the material, and ultimately, on the applied stress. Relaxing the assumption that the particles are infinitely rigid compared to the matrix and accounting for their finite stiffness, we subsequently apply the Mori–Tanaka approach to specify the interfacial and matrix stresses.

2. Analysis

2.1. Homogenization and stress analysis of particulate linearly-elastic composite material

The methods of homogenization of materials with inclusions, such as particulate and fibrous composites, include the Halpin–Tsai method, the self-consistent method, the Mori–Tanaka model, the double-inclusion method, the models of Ponte Castaneda and Willis, the Kuster–Toksoz model, etc. Besides these methods, bounding techniques for the tensor of stiffness have been suggested by Hashin and Shtrikman, Beran, Molyneux and McCoy, Gibiansky and Torquato. Among reviews of the homogenization techniques, mentioned are [3,5,2,22].

The Mori–Tanaka method [19,20] adopted in the present study expands Eshelby's technique for the dilute equivalent inclusion [23] accounting for the finite concentration of inclusions (fibers or particles). This is achieved by assumption that the average strain in the individual inclusion is related to the average strain in the matrix by the same strain concentration Eshelby's tensor that relates the strain in a dilute inclusion to the applied strain. Subsequent derivations of the tensor of stiffness are well known and the results are reproduced here for completeness and because they should be employed in the stress and fracture analyses. In the case of spherical inclusions, the stiffness evaluated by this method coincides with Hashin–Shtrikman lower bound.

The relevant approach to the evaluation of local stresses in the phases of the composite material was developed by Tandon and Weng [24] concentrating on the stresses at the interface of the spheroidal inclusion and the stresses in the matrix, just outside the inclusion. This solution utilized the jump condition across the interface formulated in [25,23] using the change in the Newtonian and biharmonic potentials across the surface with the jump in density. The solution developed in [24] was later found in compliance with the results generated by the finite element analysis [26] and applied to the analysis of shape memory alloy inclusions in an elastic matrix [27].

The constitutive relationship for a linearly elastic composite medium relating the tensors of applied stress and average strain is

$$\bar{\boldsymbol{\sigma}}_{\mathbf{o}} = \mathbf{L}\bar{\boldsymbol{\varepsilon}}_{\mathbf{o}} \tag{1}$$

where $\mathbf{L}$ is the tensor of stiffness of the composite medium obtained through an appropriate homogenization procedure.

According to Hill [28], the tensor of stiffness of a material with embedded inclusions can be represented as

$$\mathbf{L} = \mathbf{L}_1 + V_2(\mathbf{L}_2 - \mathbf{L}_1)\mathbf{A} \tag{2}$$

where $\mathbf{L}_i$ is the stiffness tensor of the ith phase (the subscripts 1 and 2 identify the matrix and inclusions, respectively), V_2 the volume fractions of the inclusions, and $\mathbf{A}$ is the strain concentration tensor representing the relationship between the tensors of average strains in inclusions $\bar{\boldsymbol{\varepsilon}}_{\mathbf{2}}$ and the tensor of mean remote applied strain $\bar{\boldsymbol{\varepsilon}}_{\mathbf{o}}$:

$$\bar{\boldsymbol{\varepsilon}}_{\mathbf{2}} = \mathbf{A}\bar{\boldsymbol{\varepsilon}}_{\mathbf{o}} \tag{3}$$

The strain concentration tensor evaluated by assumptions of the Mori–Tanaka theory is expressed in terms of the Eshelby's strain concentration tensor for the dilute problem as

$$\mathbf{A} = \mathbf{A}_{Eshelby}(V_1\mathbf{I} + V_2\mathbf{A}_{Eshelby})^{-1} \tag{4}$$

where $\mathbf{I}$ is the identity tensor and the Eshelby strain concentration tensor is

$$\mathbf{A}_{Eshelby} = [\mathbf{I} + \mathbf{S}\mathbf{L}_1^{-1}(\mathbf{L}_2 - \mathbf{L}_1)]^{-1} \tag{5}$$

The elements of the Eshelby tensor $\mathbf{S}$ depend on the inclusion aspect ratio and elastic constants of the matrix [24]; they are reproduced for the case of spherical inclusions in Appendix A.

The combination of Eqs. (2), (4), and (5) yields the tensor of stiffness:

$$\mathbf{L} = \mathbf{L}_1 + V_2(\mathbf{L}_2 - \mathbf{L}_1)\mathbf{T}(V_1\mathbf{I} + V_2\mathbf{T})^{-1}, \quad \mathbf{T} = \mathbf{A}_{Eshelby} \tag{6}$$

The explicit form of the constitutive equations for the case of spherical particles is [29]:

$$\begin{aligned} K &= K_1 + \frac{V_2(K_2 - K_1)}{1 + V_1\frac{K_2 - K_1}{K_1 + 1.333\mu_1}} \\ \mu &= \mu_1 + \frac{V_2(\mu_2 - \mu_1)}{1 + V_1\frac{\mu_2 - \mu_1}{\mu_1 + f_1}} \end{aligned} \tag{7}$$

where K and μ denote the bulk and shear moduli, respectively, and $V_1 = 1 - V_2$ is the volume fraction of the matrix. The coefficient f_1, the modulus of elasticity of the homogeneous isotropic composite E and its Poisson ratio ν are

$$\begin{aligned} f_1 &= \frac{\mu_1(9K_1 + 8\mu_1)}{6(K_1 + 2\mu_1)} \\ K &= \frac{E}{3(1 - 2\nu)} = \frac{E\mu}{3(3\mu - E)} \end{aligned} \tag{8}$$

The stress analysis includes finding the stresses at the critical locations where the initial damage can originate. These locations are likely to be the interface between the matrix and inclusion and in the matrix, just outside the inclusion. The concentration on these stresses is justified by experimental research demonstrating that the initial damage in composites with spherical particles subject to uniaxial tension often originates at the apex of a particle

[12]. The exact location of the damage, i.e. the coordinates of the largest stresses on the spherical interface and in the adjacent matrix can be predicted using the solution [24].

Consider a particulate material with spherical particles subject to uniaxial stress σ_∞. The coordinate system and the applied stress are shown in Fig. 1. The stresses in the matrix, just outside the spherical particle, are [24]:

$$\begin{aligned}
\sigma_{11} &= \sigma_\infty\left[1+\frac{V_1(b_1p_1+2b_2p_2)}{(1+\nu_1)(1-2\nu_1)}+\frac{p_1\cos^2\theta+p_2(\nu_1+\sin^2\theta)}{1-\nu_1^2}\cos^2\theta\right]\\
\sigma_{22} &= \sigma_\infty\left[\frac{V_1(b_3p_1+(b_4+b_5)p_2)}{(1+\nu_1)(1-2\nu_1)}+\frac{p_1\cos^2\theta+p_2(\nu_1+\sin^2\theta)}{1-\nu_1^2}\sin^2\theta\right]\\
\sigma_{33} &= \sigma_\infty\left[\frac{V_1(b_3p_1+(b_4+b_5)p_2)}{(1+\nu_1)(1-2\nu_1)}+\frac{\nu_1p_1\cos^2\theta+p_2(1+\nu_1\sin^2\theta)}{1-\nu_1^2}\right]\\
\sigma_{12} &= -\sigma_\infty\frac{p_1\cos^2\theta+p_2(\nu_1+\sin^2\theta)}{1-\nu_1^2}\sin\theta\cos\theta
\end{aligned} \tag{9}$$

The coefficients b_j and p_j are specified in [24] in terms of the elements of Eshelby's tensor (for completeness, these coefficients are provided in Appendix A).

The interfacial stresses are

$$\begin{aligned}
\sigma_{11}^{(\text{inter})} &= \sigma_\infty\left[\frac{p_1\cos^2\theta+p_2(\nu_1+\sin^2\theta)}{1-\nu_1^2}\cos^2\theta\right]\\
\sigma_{22}^{(\text{inter})} &= \sigma_\infty\left[\frac{p_1\cos^2\theta+p_2(\nu_1+\sin^2\theta)}{1-\nu_1^2}\sin^2\theta\right]\\
\sigma_{33}^{(\text{inter})} &= \sigma_\infty\left[\frac{\nu_1p_1\cos^2\theta+p_2(1+\nu_1\sin^2\theta)}{1-\nu_1^2}\right]\\
\sigma_{12}^{(\text{inter})} &= -\sigma_\infty\frac{p_1\cos^2\theta+p_2(\nu_1+\sin^2\theta)}{1-\nu_1^2}\sin\theta\cos\theta
\end{aligned} \tag{10}$$

The stresses given by (10) can be used to assess the bonding strength between the particle and matrix. If necessary, this strength can be increased treating the particles with silane coupling agent (e.g., [30]).

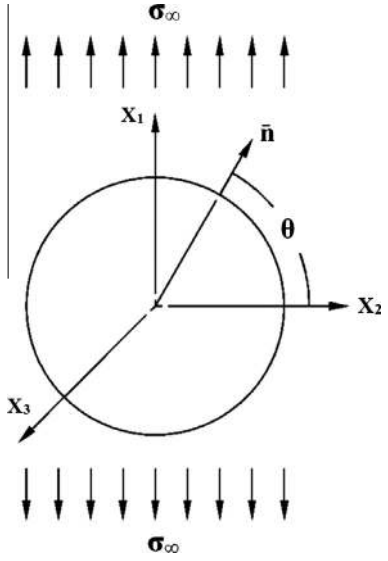

Fig. 1. Problem formulation and coordinate system: a spherical particle surrounded by matrix and subjected to uniaxial stresses.

2.2. Observation on resilience and fracture of particulate composite with spherical particles

The resilience of the material is defined as the amount of energy absorbed prior to the onset of a physically nonlinear behavior. While the resilience differs from toughness, it is a useful indicator of the energy absorption capacity prior to initial failure. In the problem under consideration the deviation from the linear elastic response is associated with the material failure in the matrix adjacent to particles or at the matrix–particle interface.

An estimate of the resilience change compared to that for the pristine matrix is possible utilizing the homogeneous model for the composite material subjected to uniaxial stress σ_∞. The homogeneous material is isotropic, its modulus of elasticity given by Eqs. (7) and (8). Although the micromechanical stresses at the RUC level are three-dimensional as reflected in Eqs. (9) and (10), the macromechanical state of stress in the homogeneous pseudo-isotropic material is one-dimensional. Accordingly, we use the ratio representing the strain energy density of the particle-reinforced composite at the applied stress corresponding to the onset of failure (U) to the energy density of matrix subjected to the uniaxial stress equal to the matrix tensile strength (U_1):

$$k=\frac{U}{U_1}=\left(\frac{E_1}{E}\right)\left(\frac{s}{s_1}\right)^2 \tag{11}$$

In Eq. (11), s_1 and E_1 are the matrix tensile strength and modulus of elasticity, respectively, and $s=\min(\sigma_\infty^{(mat)},\ \sigma_\infty^{(\text{inter})})$ is the smaller of the applied stress corresponding to the onset of failure in the matrix and its counterpart resulting in the failure of the interface (the strength of particles is assumed to exceed s).

As follows from the cited above experiments [12], the failure in particulate composites often starts with the loss of strength at the matrix–particle interface at the apex of the particle, followed with the initial propagation of the debonding crack along a part of the interface. Subsequently, the crack kinks from the interface and propagates in the matrix. The kinking angle observed was in the range from 40° to 45°, so that the analysis should be conducted by assumption of a mixed mode of fracture. Therefore, while the solution in the previous section enables us to estimate the applied stress corresponding to the onset of damage and its location (as shown in examples, our analysis for the alumina–polyurethane composite confirms the location of damage predicted for other materials in [12]), the subsequent problem is that of debonding and matrix fracture in the particulate composite medium.

We discuss here the approach to the fracture problem distinguishing between microfracture that occurs at the particle–matrix interface, mesofracture concerned with the propagation of the crack in the matrix of RUC after kinking off the interface and macrofracture, i.e. cracking on the scale exceeding that of RUC. The debond microcrack fracture problem is most challenging since it requires the analysis of a crack at the spherical interface of dissimilar materials, an estimate of the conditions of its propagation along the interface, and establishing of the conditions for kinking off the spherical interface. Such micromechanical fracture analysis is further complicated due to rapidly changing with coordinates three-dimensional microstresses at the interface as well as in the adjacent matrix and in the region of the particle adjacent to the crack. These microstresses cannot be estimated for the intact RUC, i.e. it is necessary to recalibrate them reflecting the progression of the debond microcrack. This implies that the solution should rely on the numerical analysis, taking into account a continuous redistribution of the local microstresses along and in the vicinity to the interface associated with the crack propagation.

Once the microcrack kinked off the damaged interface, its propagation within the matrix of RUC occurs at an angle that is

governed by the local stress tensor. The stresses in the matrix surrounding the particle vary with coordinates, even before the damage is inflicted. As the crack propagates in the matrix, the local stiffness around the crack changes resulting in additional local stress redistribution. Accordingly, classical methods of the analysis of mixed-mode fracture are not suitable in the mesofracture problem, except for a simplified first-approximation analysis relying on average stresses in the matrix evaluated by the Mori–Tanaka approach. In such simplified analysis, the average stress tensor in the matrix is available using the average matrix strains multiplied by the stiffness tensor of the matrix:

$$\bar{\boldsymbol{\sigma}}_1 = \mathbf{L}_1 \bar{\boldsymbol{\varepsilon}}_1$$

$$\bar{\boldsymbol{\varepsilon}}_1 = \frac{1 - V_2 \mathbf{A}}{1 - V_2} \bar{\boldsymbol{\varepsilon}}_0 \tag{12}$$

where the tensor of average strain in the matrix is obtained using the rule of mixtures for the strains and Eq. (3). The applicability of Eq. (12) to a first-order approximation of mesofracture can be established only upon the comparison of the results generated by this equation with a numerical analysis that is preferred for this problem.

Due to variations of local stresses in the matrix, the orientation of the mesocrack can change one or several times during its propagation within RUC. Accordingly, the numerical procedure monitoring mesofracture has to be "incremental," both the orientation of the crack and the conditions of its propagation being inspected at each step. The situation is demonstrated in Fig. 2 where the pre-existing crack at the angle ψ in the x_1–x_2 coordinate system changes its orientation. The analysis should employ local stresses evaluated at the previous step of the analysis to specify both the new angle as well as the conditions of the further crack propagation. While the problem is three-dimensional, certain simplifications can be employed enabling us to adopt available criteria for the mixed-mode fracture as discussed below.

Considering the crack propagating in the x_1–x_2 plane the effect of stresses σ_{33} on fracture can be neglected. This enables us to apply the plane-stress mixed-mode fracture criteria that have been analyzed in a number of studies [31,32]. The contemporary criteria usually disregard the effect of so-called T-stresses oriented along the axis of the crack (for examples of solutions incorporating these stresses, see [33,34]). With these simplifications, we can adopt the maximum hoop stress criterion of Erdogan and Sih [35] that was shown accurate in the analysis of mixed-mode crack growth and orientation [32].

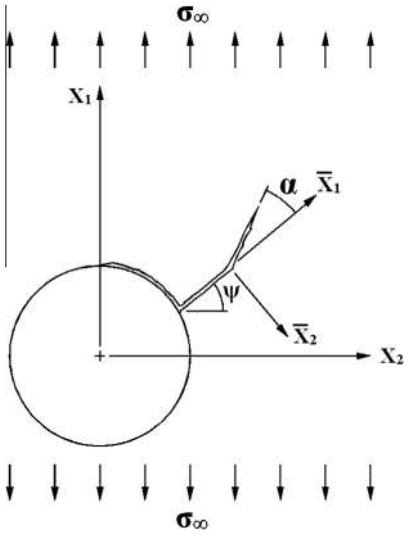

Fig. 2. Crack propagating in the matrix after kinking off the particle–matrix interface (coordinate systems and orientation).

Let us assume that we know the state of stresses and the orientation of the crack from the previous step of the numerical analysis accounting for effects of both the debond crack as well as the crack in the matrix. Then at the current step we can start with known angle of the crack ψ and the local tensor of stress in the $\bar{x}_1 - \bar{x}_2$ coordinate system (Fig. 2)

$$\boldsymbol{\sigma}_1(\bar{X}) = \left\{ \begin{array}{c} \sigma_{\bar{x}_1\bar{x}_1}(\bar{X}) \\ \sigma_{\bar{x}_2\bar{x}_2}(\bar{X}) \\ \sigma_{\bar{x}_1\bar{x}_2}(\bar{X}) \end{array} \right\} \tag{13}$$

where $\bar{X}$ is a position vector of the tip of the crack.

The solution presented in [35,36] defines both the angle of the further crack propagation counted from the $\bar{x}_1$ axis (α) as well as the condition of propagation in terms of the Mode I fracture toughness of matrix (K_{I1}) and the Modes I and II stress intensity factors in the $\bar{x}_1 - \bar{x}_2$ coordinates:

$$\begin{aligned} &\sin\alpha + (3\cos\alpha - 1)\cot\psi = 0 \\ &\left(\cos\frac{\alpha}{2}\right)\left[K_I \cos^2\frac{\alpha}{2} - \frac{3}{2}K_{II}\sin\alpha\right] = K_{I1} \end{aligned} \tag{14}$$

Macrofracture, i.e. the propagation of a "mature" crack whose length exceeds the size of RUC within the particulate material is affected by particles encountered by the crack. The phenomena occurring as a result of the presence of the particles include crack shielding, crack deflection, trapping and crack face bridging; the review of these effects can be found in [18,17,37].

Although a comprehensive analysis of macrofracture in particulate composites is outside the scope of this paper, the recommendations for two particular cases suggested in [18] are useful in numerous situations. In particular, if the particles are much tougher than the matrix, i.e. $K_p/K_m > 7$ (K_p is the toughness of particles, K_m is the toughness of matrix), the toughness of the particular composite is approximated by

$$K = 3.09\frac{R}{L}K_p \tag{15}$$

where R and L are the radius of the particle and the spacing between the centers of particles, respectively (note that $R/L = \sqrt{V_2/\pi}$ and the equation above applies only if $R/L < 0.25$). The mechanism of fracture in this case involves pinning of the crack by intact particles in its wake. On the other hand, if the toughnesses of particles and matrix are comparable, i.e. $K_p/K_m < 3$, the particles are penetrated by the expanding crack. In such situation, for the entire spectrum of the ratio R/L,

$$K = K_m\left\{1 + \frac{2R}{L}\left[\left(\frac{K_p}{K_m}\right)^2 - 1\right]\right\}^{\frac{1}{2}} \tag{16}$$

In the materials considered in numerical examples, alumina powder (nanoparticles) are embedded in the polyurethane matrix. The toughness of alumina was estimated at $K_p = 4.0\ \text{MPa} \times \text{m}^{1/2}$ [38]. A typical toughness of polyurethane is in the range from $K_m = 1.0\ \text{MPa} \times \text{m}^{1/2}$ to $K_m = 2.0\ \text{MPa} \times \text{m}^{1/2}$ [39]. Therefore, Eq. (16) may be to predict macrofracture in the alumina-reinforced particulate composites. For example, if $K_p/K_m = 3$, toughness of the particulate material increases from that of the pristine matrix ($V_2 = 0$) to 2.44 times the pristine matrix toughness for $V_2 = 0.3$.

2.3. Stress analysis of particulate composite consisting of incompressible hyperelastic matrix and stiff particles

Consider the case where deformations are sufficiently large to justify the analysis modeling the matrix as a hyperelastic material.

The approach utilizes an expansion of the Mori–Tanaka analysis with the matrix being represented by a quasi-linear elastic model whose "tangential" properties depend on the strain. The steps of the proposed analytical approach are outlined below:

a. Employing the theory of incompressible hyperelastic elastomers with rigid particles [6] we derive the tangential stiffness tensor of the composite material.
b. We determine the tangential stiffness tensor of the incompressible hyperelastic matrix from the tangential stiffness tensor of the composite material.
c. Abandoning the assumption that the particles are "rigid," we employ the Mori–Tanaka theory to trace the process of accumulation of stresses in the elements of the particulate composite as a function of the increasing axial strain (and accordingly, as a function of the applied stress).

The solution utilizes the Mori–Tanaka theory in parts "b" and "c." The following assumptions are added to those of the Mori–Tanaka theory:

a. The matrix material is incompressible (this is acceptable for numerous elastomers). The implication for the particulate composite with rigid particles is that such material is also incompressible.
b. The effect of finite stiffness of particles on the overall stiffness of the particulate material can be discounted treating them as "rigid" compared to the matrix.

Consider an incompressible hyperelastic material. Contrary to compressible materials possessing two independent engineering constants, the Poisson ratio of incompressible materials is defined being equal to 0.5. Accordingly, only one of the engineering constants of an incompressible material is independent and can be specified from the single test, such as uniaxial tension.

According to numerous theories of hyperelastic materials, the strain energy density is expressed in terms of the invariants of the deformation tensor that is defined in terms of deformation gradients, i.e.

$$\mathbf{B} = \mathbf{F}\cdot\mathbf{F}^T, \quad B_{ij} = F_{in}F_{jn}, \quad F_{in} = \delta_{in} + u_{i,n} \tag{17}$$

where δ_{in} is the Kroneker's delta and $u_{i,n}$ is a derivative of the displacement in the ith direction with respect to the nth coordinate.

The invariants of the deformation tensor in terms of the principal stretches λ_i are

$$\begin{aligned} I_1 &= tr(\mathbf{B}) = B_{ii} = \lambda_1^2 + \lambda_2^2 + \lambda_3^2, \\ I_2 &= \frac{1}{2}[I_1^2 - tr(\mathbf{B}^2)] = \frac{1}{2}[I_1^2 - B_{in}B_{ni}] = \lambda_1^2\lambda_2^2 + \lambda_2^2\lambda_3^2 + \lambda_1^2\lambda_3^2, \\ I_3 &= \det(\mathbf{B}) = \lambda_1^2\lambda_2^2\lambda_3^2 \end{aligned} \tag{18}$$

In an incompressible material $I_3 = 1$ and given the principal stretch λ_1 found in a uniaxial tension test $\lambda_2 = \lambda_3 = \lambda_1^{-2}$.

The tensor of true (Cauchy) stress is obtained as [40]:

$$\boldsymbol{\sigma} = 2\frac{dU}{dI_1}\mathbf{B} - p\mathbf{I} \tag{19}$$

where, as above, U is the strain energy density and p is the additional pressure that should be applied to satisfy the boundary conditions.

In the case of a neo-Hookean material subject to a uniaxial tension, the true stress is the following function of the maximum principal stretch in the loading direction (e.g., [6]):

$$\bar{\sigma}_1 = \mu_1(\lambda_1^2 - \lambda_1^{-1}) \tag{20}$$

where μ_1 is the shear modulus of the material (shear modulus of matrix at small strains). The overbar in Eq. (20) distinguishes the Cauchy stress from the nominal (engineering) stress.

Accounting for the amplification of the first invariant of the deformation tensor associated with the Mullins effect at large strains, Bergstrom and Boyce [6] suggested the following relationship for an elastomer with rigid inclusions:

$$\bar{\sigma}_1 = \mu_1(1 - V_2)[1 + 3.5V_2 + 30V_2^2](\lambda_1^2 - \lambda_1^{-1}) \tag{21}$$

Using the relationship between the uniaxial true and nominal stresses

$$\bar{\sigma}_1 = \lambda_1\sigma_1 \tag{22}$$

the tangent stiffness of the elastomer with "rigid" inclusions is available from (21). The principal stretch is related to the axial composite strain and its increment by $\varepsilon_1 = \lambda_1 - 1$, $d\varepsilon_1 = d\lambda_1$. Accordingly, the tangent modulus of elasticity of the incompressible material can be found calculating the stresses from the nominal stress–stretch relationship obtained from Eqs. (21) and (22):

$$E(\hat{\varepsilon}_1) = \left(\frac{d\sigma_1}{d\varepsilon_1}\right)_{\hat{\varepsilon}_1} = \mu_1(1 - V_2)[1 + 3.5V_2 + 30V_2^2](1 + 2\hat{\lambda}_1^{-3}) \tag{23}$$

where $\hat{\lambda}_1 = \hat{\varepsilon}_1 + 1$ and $\hat{\varepsilon}_1$ are the stretch and strain corresponding to the current value of the tangent modulus.

Knowing the value of the tangent modulus of elasticity and using the Poisson ratio of the incompressible material that is independent of the strain and equals to $\nu = 0.5$, the shear modulus of the particulate composite is available as $\mu(\hat{\varepsilon}_1) = \frac{1}{3}E(\hat{\varepsilon}_1)$.

The previous analysis demonstrates the evaluation of the tangent stiffness tensor of the incompressible hyperelastic matrix with "rigid" inclusions. Following the approach outlined above, the finite stiffness of the inclusions can now be accounted for and the micromechanical equations employed to evaluate the tangent stiffness tensor of the matrix from the tangent stiffness tensor of the composite and the stiffness tensor of the inclusions. According to such approach, the tensor of stiffness of a composite material becomes

$$\mathbf{L}(\hat{\varepsilon}_1) = \mathbf{L}_1(\hat{\varepsilon}_1) + V_2[\mathbf{L}_2 - \mathbf{L}_1(\hat{\varepsilon}_1)]\mathbf{T}(\hat{\varepsilon}_1)[V_1\mathbf{I} + V_2\mathbf{T}(\hat{\varepsilon}_1)]^{-1} \tag{24}$$

where the tensor of stiffness in the left side is already determined and the tensor of stiffness of the particles $\mathbf{L}_2$ is known and independent of the applied strain. Accordingly, the tangent tensor of stiffness of the matrix, i.e. $\mathbf{L}_1(\hat{\varepsilon}_1)$, can be derived from Eq. (24). The Eshelby strain concentration tensor in Eq. (24) is

$$\mathbf{T}(\hat{\varepsilon}_1) = [\mathbf{I} + \mathbf{S}\mathbf{L}_1^{-1}(\hat{\varepsilon}_1)(\mathbf{L}_2 - \mathbf{L}_1(\hat{\varepsilon}_1))]^{-1} \tag{25}$$

The elements of the Eshelby tensor are dependent on the particle aspect ratio and the Poisson ratio of the matrix that is equal to 0.5 since the matrix material is incompressible.

Finding tensor $\mathbf{L}_1(\hat{\varepsilon}_1)$ from Eqs. (24) and (25) is a challenging problem. Accordingly, we retain the assumption that the particles are rigid at the phase of the analysis. Then if the matrix is incompressible, Eqs. (7) and (8) yield the tangent shear modulus of the matrix:

$$\mu_1(\hat{\varepsilon}_1) = \frac{\mu(\hat{\varepsilon}_1)}{1 + \frac{5}{2}\frac{V_2}{V_1}} \tag{26}$$

Subsequently, the tangent elastic modulus of the matrix is found from $E_1(\hat{\varepsilon}_1) = 3\mu_1(\hat{\varepsilon}_1)$.

The analysis of stresses as functions of the applied strain can now be conducted using the tangential properties of the matrix and elastic properties of particles by Eqs. (9) and (10) for the matrix, just outside the particles, and at the interface, respectively. The analysis should start with small values of the strain $\hat{\varepsilon}_1$, gradually increasing it and finding the corresponding increments of

stresses. In general, the tensor of stress $\boldsymbol{\sigma}$ at the applied strain $(\hat{\varepsilon}_1 + d\hat{\varepsilon}_1)$ is evaluated from:

$$\boldsymbol{\sigma}(\hat{\varepsilon}_1 + d\hat{\varepsilon}_1) = \boldsymbol{\sigma}(\hat{\varepsilon}_1) + d\boldsymbol{\sigma}(d\hat{\varepsilon}_1) \tag{27}$$

where $d\hat{\varepsilon}_1$ is an increment of the axial strain in the composite material. The expressions for the increments of the stresses in the matrix, just outside the particles, and at the interface are shown in Appendix B. Using the formulas for the stresses requires us to specify the applied axial stress, rather than the axial strain in the composite material. In the case of a uniaxial loading, this stress is $\sigma_\infty(\hat{\varepsilon}_1) = E(\hat{\varepsilon}_1)\hat{\varepsilon}_1$.

3. Numerical examples

Numerical examples are concerned with the effect of alumina particles on the stresses and strength of polyurethane matrix. The properties of polyurethane are $E = 2.50$ GPa, $G = 0.938$ GPa, while those of the particles are $E = 68.9$ GPa, $G = 25.9$ GPa. The critical locations where failure can originate are the interface and the matrix adjacent to the particle that experiences stress concentration. The following results concentrate on the stresses at both these locations.

The distributions of axial stresses in the matrix, just outside the particle, normalized with respect to the applied stress are demonstrated in Figs. 3–5. The shear stresses in the matrix adjacent to the particle are presented in Fig. 6. The shear stresses in the particle being absent at the uniaxial loading considered in the examples, the stresses shown in Fig. 6 coincide with the shear stresses at the interface. In agreement with the observations of Tandon and Weng [24], the largest axial stress σ_{11} reaches the maximum value at the angular location about 30° from the apex, the coordinate of the latter being $\theta = 90°$ (Fig. 3). However, this stress experiences relatively small variations in the interval $60° \leqslant \theta \leqslant 90°$ This may justify the use of the approximate stress concentration factor evaluated using the stress at the apex in the case where the stiffness of the particles is at least one order of magnitude higher than that of the matrix [41]:

$$\sigma_{11}^{\max} = \left(\frac{2}{1+\nu_1} + \frac{1}{4-5\nu_1}\right)\sigma_\infty$$

The formula presented above is limited to the dilute case, i.e. it cannot be used if the particle volume fraction exceeds several percent.

The stress distributions in Figs. 3–6 and in the subsequent figures cover the range from the single (dilute) particle ("0% inclusions") to the particle volume fraction equal to 30%. As follows from the figures, a higher particle concentration results in a reduction of stresses in the matrix. This is anticipated since increasing the particle content reduces the stiffness mismatch between the

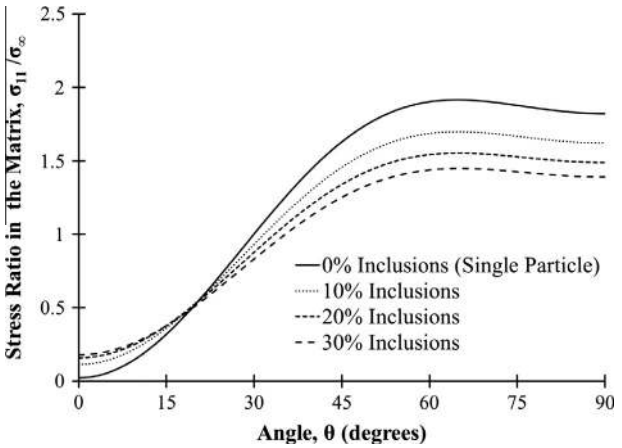

Fig. 3. Stress in the axial (x_1) direction in the matrix, just outside the particle, normalized with respect to the applied stress as the function of particle volume fraction and angular coordinate.

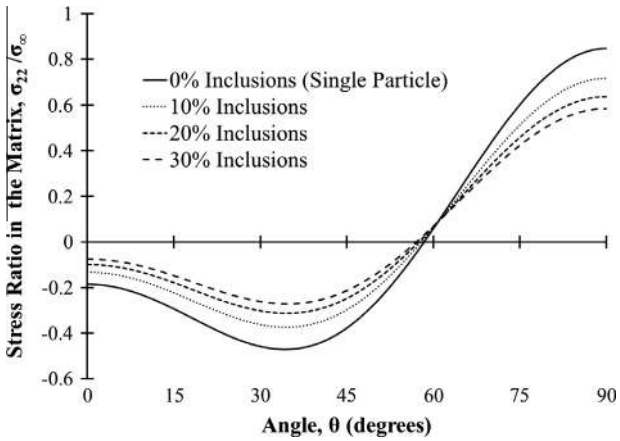

Fig. 4. Stress in the x_2-direction in the matrix, just outside the particle, normalized with respect to the applied stress as the function of particle volume fraction and angular coordinate.

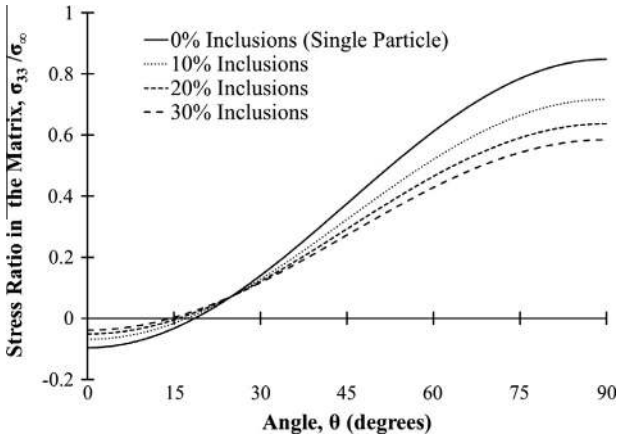

Fig. 5. Stress in the x_3-direction in the matrix, just outside the particle, normalized with respect to the applied stress as the function of particle volume fraction and angular coordinate.

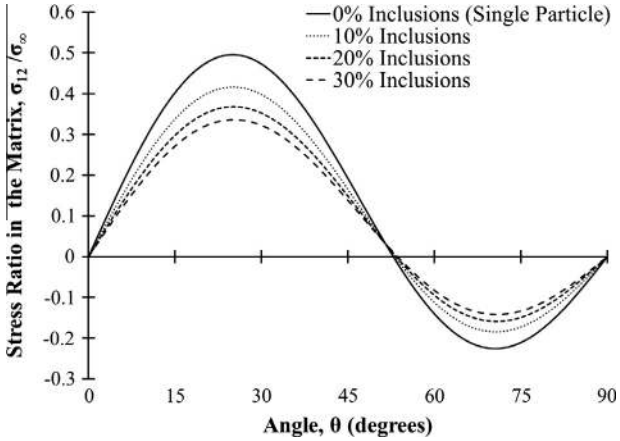

Fig. 6. Shear stress in the matrix, just outside the particle, normalized with respect to the applied stress as the function of particle volume fraction and angular coordinate.

individual particle and the surrounding homogeneous material consisting of the pristine matrix and particles resulting in a reduction of the stress concentration. The stress distribution around the particle circumference remains consistent at all particle volume fractions.

The strength of the matrix being analyzed by one of the strength criteria, the principal and von Mises stresses represent a particular interest. These normalized stresses are shown in Figs. 7 and 8, respectively. The maximum by absolute value principal stress occurs at about the same location as the maximum axial stress σ_{11}. However, the von Mises stress being a little smaller than the maximum principal stress reaches the maximum value at the angular coordinate close to $\theta = 40°$.

The distribution of the axial stresses at the interface is shown in Figs. 9–11 (as indicated above, the shear stress is given in Fig. 6). Qualitatively, these distributions are in agreement with the results presented for different materials in [24,26]. Similar to the observation made above for the matrix, the stresses decrease at a higher particle volume fraction. However, the most vulnerable locations around the interface are the apex $\theta = 90°$ and the point $\theta = 0°$. This observation is confirmed by the results both for the maximum principal stress (Fig. 12) as well as for the von Mises stress (Fig. 13). The values of the maximum principal stress and the maximum von Mises stress in the matrix outside the particle and at the interface are close, although the locations of these stresses differ. It may be concluded that a rational design can be achieved if the strength of the interface is close to that of the matrix.

The effect of the stiffness of the matrix on the maximum principal stress and on the von Moses stress in the matrix, just outside the particle, and at the interface is shown in Figs. 14–21. The first four figures (Figs. 14–17) demonstrate this effect for the dilute problem, while the second set (Figs. 18–21) present the case of the particle volume fraction equal to 30%. As follows from these figures, the locations of the maximum principal and the von Mises stresses both in the matrix and at the interface remain consistent for a broad range of matrix stiffness. The beneficial effect of a stiffer matrix on the stresses that has already been mentioned is clearly demonstrated in Figs. 14–21.

An estimate of the resilience of the material is presented here for the case where the matrix fails prior to the interface (this may be the case if the strength of the interface is enhanced by special treatments [30]). The ratio of the modulus of elasticity of the particulate composite to that of the matrix varies from 1.0 to approximately 1.8 as the particle volume fraction increases from 0% to 30% [1]. The stress ratio in Eq. (11) reflecting the strength of the matrix and utilizing the maximum principal stress criterion

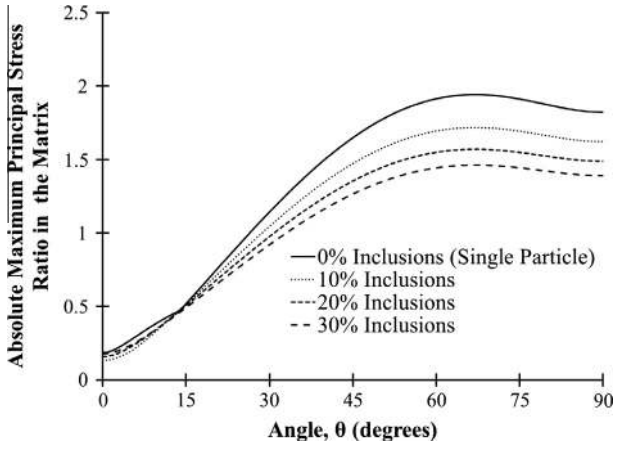

Fig. 7. Maximum principal stress in the matrix, just outside the particle, normalized with respect to the applied stress as the function of particle volume fraction and angular coordinate.

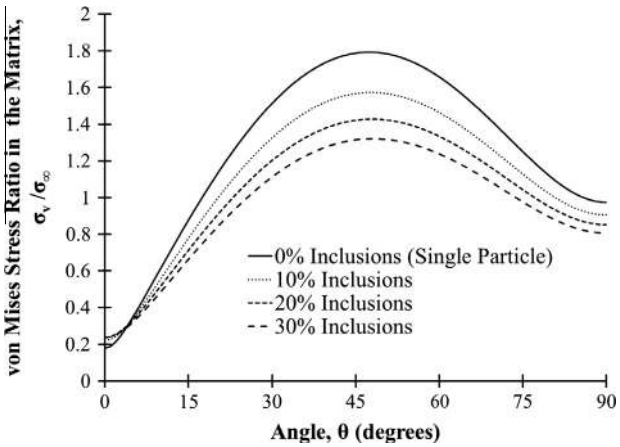

Fig. 8. The von Mises stress in the matrix, just outside the particle, normalized with respect to the applied stress as the function of particle volume fraction and angular coordinate.

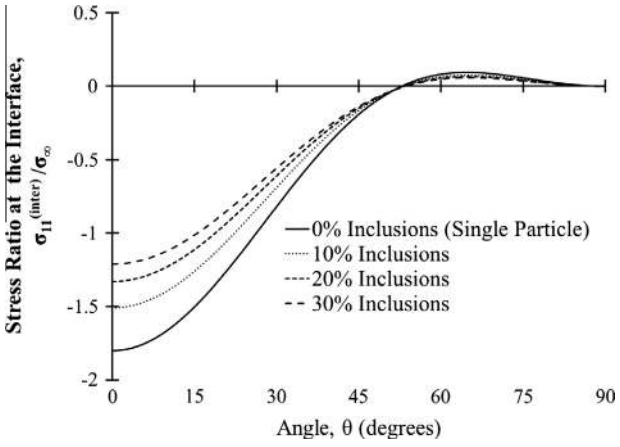

Fig. 9. Stress in the axial (x_1) direction at the interface normalized with respect to the applied stress as the function of particle volume fraction and angular coordinate.

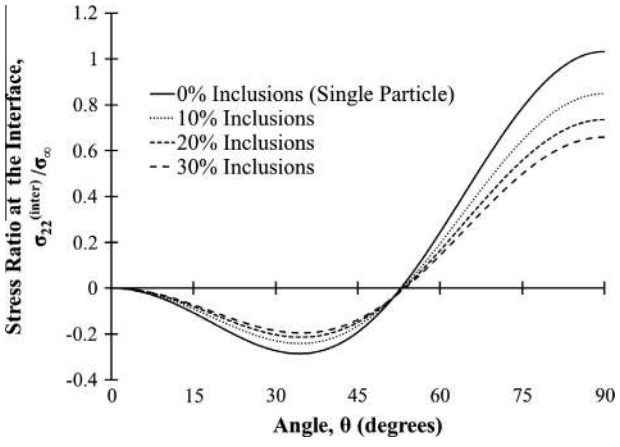

Fig. 10. Stress in the x_2-direction at the interface normalized with respect to the applied stress as the function of particle volume fraction and angular coordinate.

varies from 1.8 (dilute model) to 1.4 (30% particle volume fraction). Accordingly, we observe that the resilience ratio k in Eq. (11) decreases from the value close to 2.0 in the dilute case approaching unity at the particle volume fraction close to 30%. Therefore, while the absorption of energy prior to initial failure is significantly

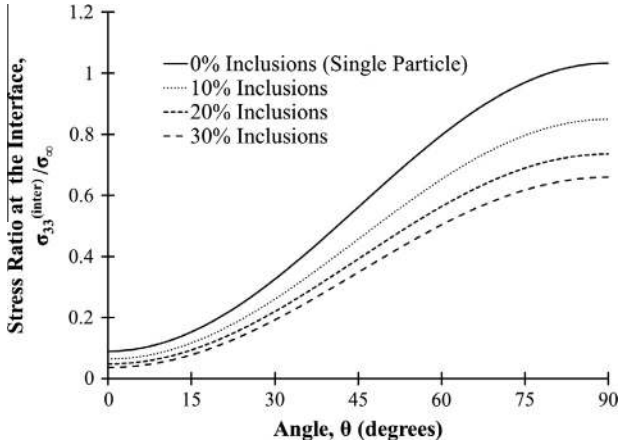

Fig. 11. Stress in the x_3-direction at the interface normalized with respect to the applied stress as the function of particle volume fraction and angular coordinate.

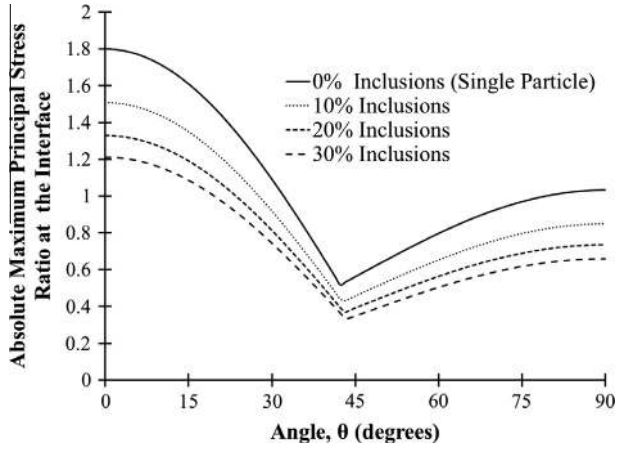

Fig. 12. Maximum principal stress at the interface normalized with respect to the applied stress as the function of particle volume fraction and angular coordinate.

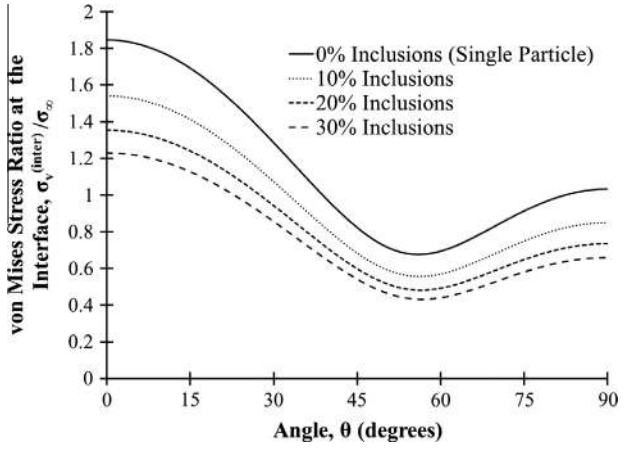

Fig. 13. The von Mises stress at the interface normalized with respect to the applied stress as the function of particle volume fraction and angular coordinate.

larger than that in the pristine matrix at a low particle concentration, it decreases and approaches unity as the density of particles increases. This is similar to a well-known negative effect of an increased stiffness on toughness of both engineering and biological materials referred to as a "banana" and "inverted banana" curves on the stiffness–toughness plane, respectively [42]. Although resilience differs from toughness for all but brittle linear elastic materials, the analogy is logical.

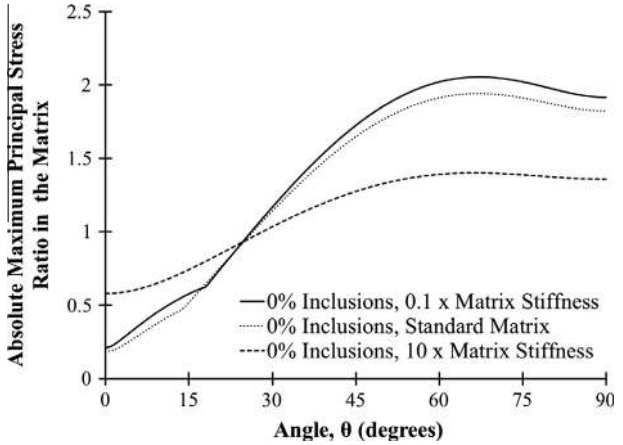

Fig. 14. Maximum principal stress in the matrix, just outside the particle, normalized with respect to the applied stress as the function of the stiffness of matrix and angular coordinate. Dilute problem: negligible particle volume fraction.

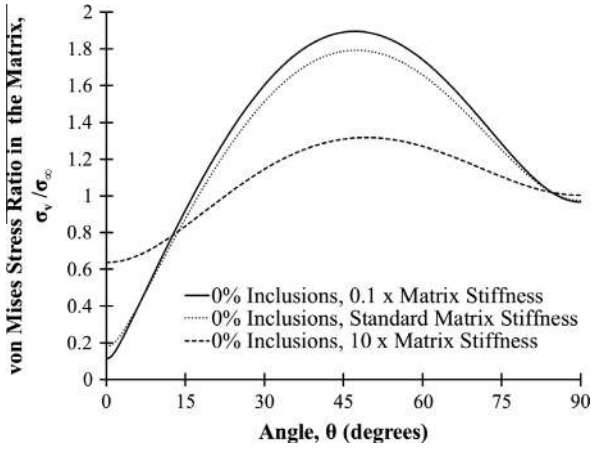

Fig. 15. The von Mises stress in the matrix, just outside the particle, normalized with respect to the applied stress as the function of the stiffness of matrix and angular coordinate. Dilute problem: negligible particle volume fraction.

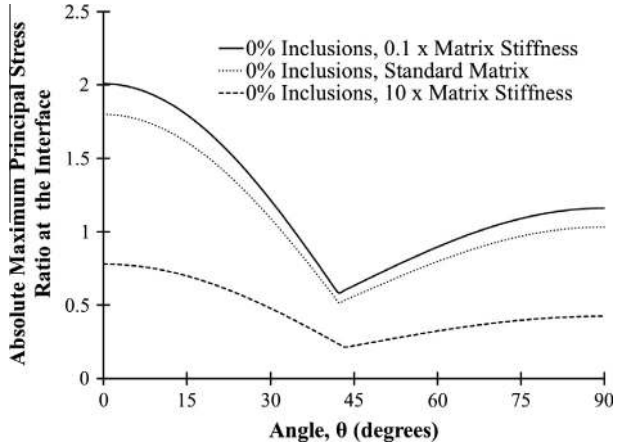

Fig. 16. Maximum principal stress at the interface normalized with respect to the applied stress as the function of the stiffness of matrix and angular coordinate. Dilute problem: negligible particle volume fraction.

4. Discussion and conclusions

The paper utilizes the stress analysis based on the Mori–Tanaka theory to elucidate the stresses in a particulate composite consisting of an elastic matrix reinforced by spherical particles and subject to uniaxial tension. The materials used in the numerical

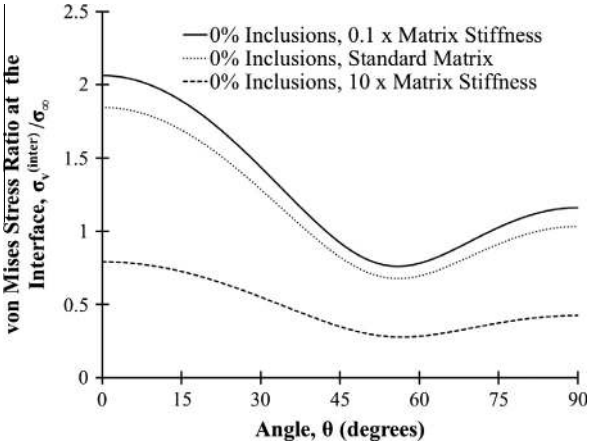

Fig. 17. The von Mises stress at the interface normalized with respect to the applied stress as the function of the stiffness of matrix and angular coordinate. Dilute problem: negligible particle volume fraction.

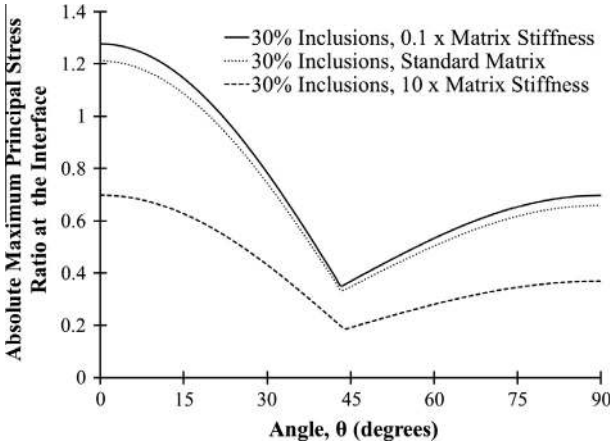

Fig. 20. Maximum principal stress at the interface normalized with respect to the applied stress as the function of the stiffness of matrix and angular coordinate. Particle volume fraction is equal to 30%.

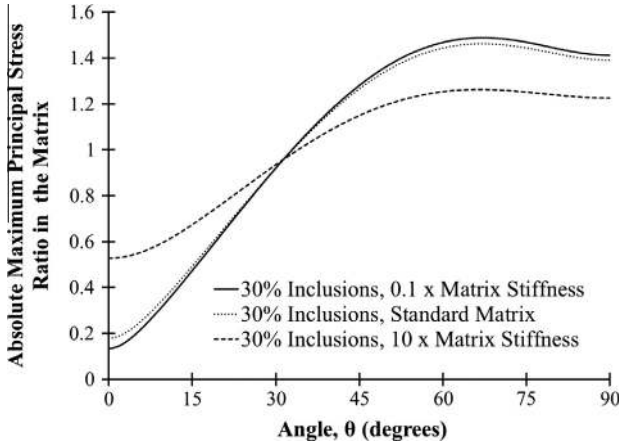

Fig. 18. Maximum principal stress in the matrix, just outside the particle, normalized with respect to the applied stress as the function of the stiffness of matrix and angular coordinate. Particle volume fraction is equal to 30%.

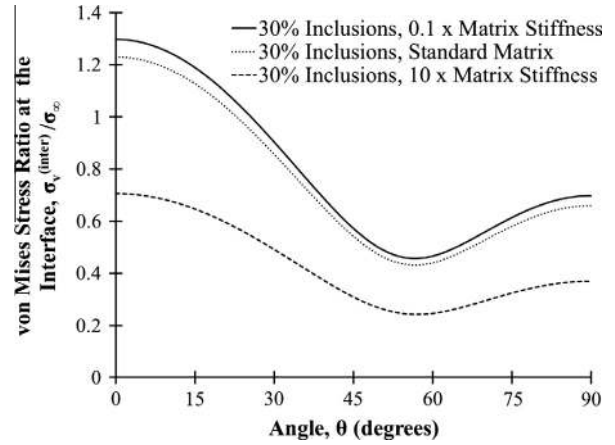

Fig. 21. The von Mises stress at the interface normalized with respect to the applied stress as the function of the stiffness of matrix and angular coordinate. Particle volume fraction is equal to 30%.

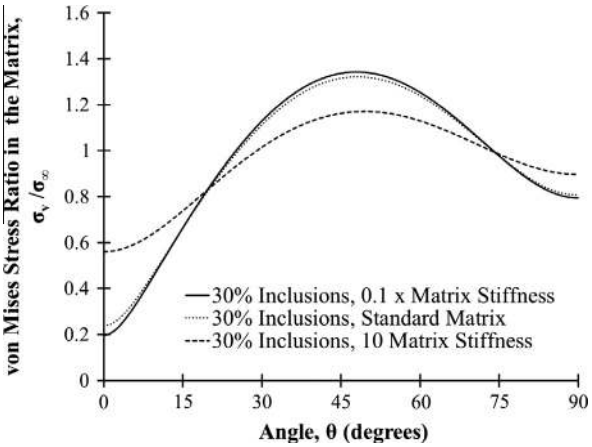

Fig. 19. The von Mises stress in the matrix, just outside the particle, normalized with respect to the applied stress as the function of the stiffness of matrix and angular coordinate. Particle volume fraction is equal to 30%.

analysis are polyurethane matrix and alumina particles. In addition to the stress analysis, the approach to the study of fracture following the initial failure in the matrix, just outside the particle, or at the particle–matrix interface is discussed.

The largest maximum principal stresses in the matrix just outside the particle occur at the angle close to $\theta = 60^\circ$ and slowly decrease toward the apex ($\theta = 90^\circ$). In the contrary, the largest von Mises stress occurs at $\theta \approx 45^\circ$. The situation is different at the interface where both the maximum absolute principal stresses as well as the largest von Mises stress occur at $\theta = 0^\circ$, the second maximum being at the apex. The order of magnitude of the highest stresses in the matrix, just outside the particle, and at the interface is the same, i.e. achieving the strength of the interface comparable to that of the matrix is highly desirable, ideally creating a system failing both in the matrix and interface at the same load (i.e. avoiding unnecessary and underutilized strength of either matrix or interface).

Increasing the volume fraction of particles results in and lower stresses both in the matrix, just outside the particles, and at the interface. Predictable, a higher stiffness of the matrix material produces the same results both in the dilute case as well as at higher particle volume fractions.

Adding particles to the matrix results in an increase in the resilience, particularly at a low particle volume fraction. However, if the volume fraction increases, the energy absorbed prior to the initial damage decreases to that for pure matrix.

Once the material fails either in the matrix adjacent to the particle or at the interface, cracks develop and fracture should be analyzed. We suggest three phases of fracture for the future research.

Microfracture involves the analysis of the crack propagating along the interface causing the initial partial or complete debonding of the particle from the matrix. The analysis of microfracture is very complicated due to the spherical shape of the interface and rapid changes of the stresses with the coordinates (i.e. an assumption of "constant" applied stresses becomes invalid at the microscale). Mesofracture at RUC level occurs in the matrix as the crack kinks off the interface and propagates in the adjacent matrix. In this case, the analysis can be conducted by a number of methods; in particular, we refer to the maximum tangential stress criterion of Erdogan and Sih. However, the stresses necessary to apply such criterion can only be accurately estimated by a numerical analysis. While microfracture and mesofracture occurring at the RUC scale require a numerical analysis, macrofracture can be studied using available analytical techniques. In particular, the effect of particles on toughness of the composite material can be evaluated by explicit formulae applicable in prescribed ranges of the particle-to-matrix toughness ratio.

The final part of the paper presents a methodology of the stress analysis of the material consisting of stiff particles embedded within an incompressible hyperelastic matrix. The stiffness analysis is conducted by modeling the particle as being "rigid" compared to the matrix, yielding the tangent stiffness tensors of the composite and the matrix. Subsequently, the finite stiffness of the particles is accounted for; this enables us to apply an incremental Mori–Tanaka technique to monitor the stresses in the material.

Acknowledgments

The authors gratefully acknowledge the financial support provided by the Missouri Department of Transportation (MoDOT) and the National University Transportation Center (NUTC) at Missouri University of Science and Technology. The conclusions and opinions expressed in this paper are those of the authors and do not necessarily reflect the official views or policies of the funding institutions.

Appendix A. Coefficients employed to evaluate the stresses according to the Mori–Tanaka theory

In the case of a uniaxial loading, the coefficients in Eqs. (9) and (10) are [24]:

$$\begin{aligned} b_1 &= 2\nu_1 S_{2211} + (1-\nu_1)(S_{1111}-1)\\ b_2 &= \nu_1(S_{2233}+S_{2222}-1) + (1-\nu_1)S_{1122}\\ b_3 &= \nu_1(S_{1111}-1) + S_{2211}\\ b_4 &= \nu_1(S_{1122}+S_{2233}) + (1-\nu_1)(S_{2211}-1)\\ b_5 &= \nu_1(S_{1122}+S_{2222}-1) + (1-\nu_1)S_{2233} \end{aligned} \tag{A1}$$

where the elements of the Eshelby tensor, in the case of spherical inclusions, are

$$\begin{aligned} S_{1111} &= S_{2222} = S_{3333} = \frac{7-5\nu_1}{15(1-\nu_1)}\\ S_{1122} &= S_{2233} = S_{3311} = \frac{5\nu_1-1}{15(1-\nu_1)}\\ S_{1212} &= S_{2323} = S_{3131} = \frac{4-5\nu_1}{15(1-\nu_1)} \end{aligned} \tag{A2}$$

The coefficients

$$\begin{aligned} p_1 &= \frac{a_1+2\nu_1 a_2}{a}\\ p_2 &= \frac{a_3-\nu_1 a_4}{a} \end{aligned} \tag{A3}$$

depend on the shear and bulk moduli of the matrix and particles and on the elements of the Eshelby tensor as follows:

$$\begin{aligned} a_1 &= V_1(S_{2222}+S_{2233}-1) + \frac{\mu_2}{\mu_2-\mu_1} + \frac{2(\mu_2K_1-\mu_1K_2)}{3(\mu_2-\mu_1)(K_2-K_1)}\\ a_2 &= V_1S_{1122} + \frac{\mu_2K_1-\mu_1K_2}{3(\mu_2-\mu_1)(K_2-K_1)}\\ a_3 &= -V_1S_{2211} - \frac{\mu_2K_1-\mu_1K_2}{3(\mu_2-\nu_1)(K_2-K_1)}\\ a_4 &= V_1(S_{1111}-1) + \frac{\mu_2}{\mu_2-\mu_1} + \frac{\mu_2K_1-\mu_1K_2}{3(\mu_2-\mu_1)(K_2-K_1)}\\ a_5 &= \left[V_1(S_{2233}-S_{2222}+1) - \frac{\mu_2}{\mu_2-\mu_1}\right]^{-1}\\ a &= -\left[V_1^2 + 2V_1\frac{\mu_1}{\mu_2-\mu_1} + \frac{\mu_1K_1}{(\mu_2-\mu_1)(K_2-K_1)}\right]\\ &\quad - V_1(S_{1111}+S_{2222}+S_{2233})\left(V_1+\frac{\mu_1}{\mu_2-\mu_1}\right)\\ &\quad - V_1^2[S_{1111}(S_{2222}+S_{2233}) - 2S_{1122}S_{2211}]\\ &\quad - \frac{\mu_2K_1-\mu_1K_2}{3(\mu_2-\mu_1)(K_2-K_1)}\left[3+V_1\begin{pmatrix}2(S_{1111}-1)+(S_{2222}+S_{2233}-1)-\\ 2(S_{1122}+S_{2211})\end{pmatrix}\right] \end{aligned} \tag{A4}$$

Appendix B. Stress increments in a composite consisting of stiff elastic spherical particles embedded within an incompressible hyperelastic matrix

The stresses in the matrix, just outside the particle, and the stresses at the particle–matrix interface can be determined using the modified solution [24]. If the composite is subject to a uniaxial loading, the increments of the stresses in the matrix, just outside the particle, at the $(k+1)$th applied stress increment $d\sigma_\infty^{(k+1)} = d\sigma_\infty(d\hat{\varepsilon}_1^{(k+1)})$ can be obtained as

$$\begin{aligned} d\sigma_{11}^{(k+1)} &= \left[1+\tfrac{V_1(b_1p_1+2b_2p_2)}{(1+\nu_1)(1-2\nu_1)} + \tfrac{p_1\cos^2\theta+p_2(\nu_1+\sin^2\theta)}{1-\nu_1^2}\cos^2\theta\right]d\sigma_\infty^{(k+1)}\\ d\sigma_{22}^{(k+1)} &= \left[\tfrac{V_1(b_3p_1+(b_4+b_5)p_2)}{(1+\nu_1)(1-2\nu_1)} + \tfrac{p_1\cos^2\theta+p_2(\nu_1+\sin^2\theta)}{1-\nu_1^2}\sin^2\theta\right]d\sigma_\infty^{(k+1)}\\ d\sigma_{33}^{(k+1)} &= \left[\tfrac{V_1(b_3p_1+(b_4+b_5)p_2)}{(1+\nu_1)(1-2\nu_1)} + \tfrac{\nu_1p_1\cos^2\theta+p_2(1+\nu_1\sin^2\theta)}{1-\nu_1^2}\right]d\sigma_\infty^{(k+1)}\\ d\sigma_{12}^{(k+1)} &= -\tfrac{p_1\cos^2\theta+p_2(\nu_1+\sin^2\theta)}{1-\nu_1^2}\sin\theta\cos\theta\, d\sigma_\infty^{(k+1)} \quad d\sigma_{13}^{(k+1)} = d\sigma_{23}^{(k+1)} = 0\\ b_i &= b_i(\sigma_\infty^{(k)} + d\sigma_\infty^{(k+1)}), \quad p_j = p_j(\sigma_\infty^{(k)} + d\sigma_\infty^{(k+1)}) \end{aligned} \tag{A5}$$

The matrix being incompressible, the Poisson ratio $\nu_1 = 0.5$. The moduli of elasticity and shear of the matrix should be evaluated at the value of the axial composite strain corresponding to the stress $(\sigma_\infty^{(k)} + d\sigma_\infty^{(k+1)})$.

The increments of the interfacial stresses at the $(k+1)$th step of uniaxial loading are (contrary to notation in Eqs. (10), the superscript "inter" is omitted):

$$\begin{aligned} d\sigma_{11}^{(k+1)} &= \left[\frac{p_1\cos^2\theta+p_2(\nu_1+\sin^2\theta)}{1-\nu_1^2}\cos^2\theta\right]d\sigma_\infty^{(k+1)}\\ d\sigma_{22}^{(k+1)} &= \left[\frac{p_1\cos^2\theta+p_2(\nu_1+\sin^2\theta)}{1-\nu_1^2}\sin^2\theta\right]d\sigma_\infty^{(k+1)}\\ d\sigma_{33}^{(k+1)} &= \left[\frac{\nu_1p_1\cos^2\theta+p_2(1+\nu_1\sin^2\theta)}{1-\nu_1^2}\right]d\sigma_\infty^{(k+1)}\\ d\sigma_{12}^{(k+1)} &= -\left[\frac{p_1\cos^2\theta+p_2(\nu_1+\sin^2\theta)}{1-\nu_1^2}\sin\theta\cos\theta\right]d\sigma_\infty^{(k+1)} \end{aligned} \tag{A6}$$

References

[1] Birman V, Chandrashekhara K, Hopkins MS, Volz JS. Effects of nanoparticle impregnation of polyurethane foam core on the performance of sandwich beams. Compos B Eng 2013;46:234–46.

[2] Tucker Iii CL, Liang E. Stiffness predictions for unidirectional short-fiber composites: review and evaluation. Compos Sci Technol 1999;59(5):655–71.
[3] Torquato S. Random heterogeneous materials: microstructure and macroscopic properties. New York: Springer; 2001.
[4] Ahmed S, Jones FR. A review of particulate reinforcement theories for polymer composites. J Mater Sci 1990;25:4933–42.
[5] Milton GW. The theory of composites. Cambridge: Cambridge University Press; 2002.
[6] Bergstrom JS, Boyce MC. Mechanical behavior of particle filled elastomers. Rubber Chem Technol 1999;72(4):633–56.
[7] Bergstrom JS, Boyce MC. Large strain time-dependent behavior of filled elastomers. Mech Mater 2000;32(11):627–44.
[8] Sahu S, Broutman LJ. Mechanical properties of particulate composites. Polym Eng Sci 1972;12(2):91–100.
[9] Lehmann B, Schlarb AK, Friedrich K, Zhang MQ, Rong MZ. Modelling of mechanical properties of nanoparticle-filled polyethylene. Int J Polym Mater 2008;57(1):81–100.
[10] Piggott MR, Leidner J. Misconceptions about filled polymers. J Appl Polym Sci 1974;18(6):1619–23.
[11] Leidner J, Woodhams RT. Strength of polymeric composites containing spherical fillers. J Appl Polym Sci 1974;18(6):1639–54.
[12] Cho J, Joshi MS, Sun CT. Effect of inclusion size on mechanical properties of polymeric composites with micro and nano particles. Compos Sci Technol 2006;66(13):1941–52.
[13] Sudduth RD. Analysis of the maximum tensile strength of a composite with spherical particulates. J Compos Mater 2006;40(4):301–31.
[14] Chan KS, Lee YD, Nicolella DP, Furman BR, Wellinghoff S, Rawls R. Improving fracture toughness of dental nanocomposites by interface engineering and micromechanics. Eng Fract Mech 2007;74(12):1857–71.
[15] Faber KT, Evans AG. Crack deflection processes-I. Theory. Acta Metall 1983;31(4):565–76.
[16] Faber KT, Evans AG. Crack deflection processes-II. Experiment. Acta Metall 1983;31(4):577–84.
[17] Suresh S. Fatigue crack deflection and fracture surface contact: micromechanical models. Metall Trans A 1985;16(2):249–60.
[18] Bower AF, Ortiz M. A three-dimensional analysis of crack trapping and bridging by tough particles. J Mech Phys Solids 1991;39(6):815–58.
[19] Mori T, Tanaka K. Average stress in matrix and average elastic energy of materials with misfitting inclusions. Acta Metall 1973;21:571–4.
[20] Benveniste Y. A new approach to the application of Mori–Tanaka's theory in composite materials. Mech Mater 1987;6(2):147–57.
[21] Genin GM, Birman V. Micromechanics and structural response of functionally graded, particulate–matrix, fiber-reinforced composites. Int J Solids Struct 2009;46(10):2136–50.
[22] Pindera MJ, Charalambakis N, Lagoudas D, Hui D. Special issue of composites Part B: homogenization and micromechanics of smart and multifunctional materials. Compos B Eng 2012;43(6):2493–4.
[23] Eshelby JD. The determination of the elastic field of an ellipsoidal inclusion and related problems. Proc Roy Soc Lond Ser A 1957;241:376–96.
[24] Tandon GP, Weng GJ. Stress distribution in and around spheroidal inclusions and voids at finite concentrations. J Appl Mech 1986;53:511–8.
[25] Mura T, Cheng PC. The elastic field outside an ellipsoidal inclusion. J Appl Mech 1977;44:591–4.
[26] Kakavas PA, Kontoni D-P. Numerical investigation of the stress field of particulate reinforced polymeric composites subject to tension. Int J Numer Methods Eng 2005;65:1145–64.
[27] Birman V. Properties and response of composite material with spheroidal superelastic shape memory alloy inclusions subject to three-dimensional stress state. J Phys D Appl Phys 2010;43(22).
[28] Hill R. Elastic properties of reinforced solids: some theoretical principles. J Mech Phys Solids 1963;11(5):357–72.
[29] Vel SS, Batra RC. Three-dimensional exact solution for the vibration of functionally graded rectangular plates. J Sound Vib 2004;272(3–5):703–30.
[30] Stewart JK, Mahfuz H, Carlsson LA. Enhancing mechanical and fracture properties of sandwich composites using nanoparticle reinforcement. J Mater Sci 2010;45(13):3490–6.
[31] Kim J-H, Paulino GH. On fracture criteria for mixed-mode crack propagation in functionally graded materials. Mech Adv Mater Struct 2007;14:227–44.
[32] Richard HA, Fulland M, Sander M. Theoretical crack path prediction. Fatigue Fract Eng Mater Struct 2005;28(1–2):3–12.
[33] Kim JH, Paulino GH. T-stress in orthotropic functionally graded materials: Lekhnitskii and Stroh formalisms. Int J Fract 2004;126(4):345–84.
[34] Ayatollahi MR, Sedighiani K. A T-stress controlled specimen for mixed mode fracture experiments on brittle materials. Eur J Mech A/Solids 2012;36:83–93.
[35] Erdogan F, Sih GC. On the crack extension in plates under plane loading and transverse shear. ASME J Basic Eng 1963;85:519–25.
[36] Sih GC. Strain–energy–density factor applied to mixed mode crack problems. Int J Fract 1974;10(3):305–21.
[37] Wetzel B, Rosso P, Haupert F, Friedrich K. Epoxy nanocomposites – fracture and toughening mechanisms. Eng Fract Mech 2006;73(16):2375–98.
[38] Casellas D, Nagl MM, Llanes L, Anglada M. Fracture toughness of alumina and ZTA ceramics: microstructural coarsening effects. J Mater Process Technol 2003;143–144(1):148–52.
[39] Fu SY, Feng XQ, Lauke B, Mai YW. Effects of particle size, particle/matrix interface adhesion and particle loading on mechanical properties of particulate–polymer composites. Compos B Eng 2008;39(6):933–61.
[40] Qi HJ, Boyce MC. Constitutive model for stretch-induced softening of the stress–stretch behavior of elastomeric materials. J Mech Phys Solids 2004; 52(10):2187–205.
[41] Goodier JN. Concentration of stress around spherical and cylindrical inclusions and flaws. Trans ASME J Appl Mech 1933;55:39–44.
[42] Qin Z, Cranford S, Ackbarow T, Buehler MJ. Robustness–strength performance of hierarchical alpha-helical protein filaments. Int J Appl Mech 2009;1(1): 85–112.